

Bitstream Collisions in Neural Image Compression via Adversarial Perturbations

Jordan Madden^{*1} Lhamo Dorje^{*1} Xiaohua Li^{*1}

Abstract

Neural image compression (NIC) has emerged as a promising alternative to classical compression techniques, offering improved compression ratios. Despite its progress towards standardization and practical deployment, there has been minimal exploration into its robustness and security. This study reveals an unexpected vulnerability in NIC - bitstream collisions - where semantically different images produce identical compressed bitstreams. Utilizing a novel whitebox adversarial attack algorithm, this paper demonstrates that adding carefully crafted perturbations to semantically different images can cause their compressed bitstreams to collide exactly. The collision vulnerability poses a threat to the practical usability of NIC, particularly in security-critical applications. The cause of the collision is analyzed, and a simple yet effective mitigation method is presented.

1. Introduction

Image compression has become crucial in today's big data regime as it enables efficient storage and transmission of image data while maintaining visual quality. Many novel media technologies such as Virtual Reality (VR), Augmented Reality (AR), Extended Reality (ER), etc. have raw data rates that are orders of magnitude above the wireless communication capacity bound, making efficient image compression especially important (Bastug et al., 2017).

In recent years, Neural Image Compression (NIC) has become popular due to its ability to outperform traditional compression techniques like JPEG (Joint Photographic Experts Group) or PNG (Portable Network Graphics) (Yang et al., 2023; Jamil et al., 2023). By leveraging the power of deep learning, NIC can optimize compression end-to-end, achieving higher compression ratios while maintaining high perceptual quality.

¹Department of ECE, Binghamton University, Binghamton, NY, USA 13902. {jmadden2,ldorje1,xli}@binghamton.edu. Correspondence to: Xiaohua Li <xli@binghamton.edu>.

submitted for review, January 2025. Copyright 2025 by the author(s).

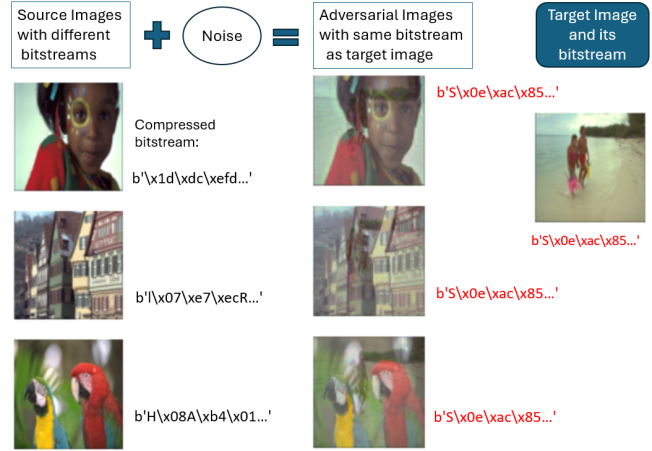


Figure 1. Bitstream collisions: Adversarial images that are perceptually different from a target image but have the same compressed bitstream as the latter.

Despite the fact that NIC algorithms are expected to be standardized and implemented in practical applications - even security-critical ones such as cryptographic protocols - their robustness and security has been largely unexplored (Liu et al., 2023; Chen & Ma, 2023). Traditional compression methods like JPEG have undergone extensive testing before real-world adoption, resulting in well-understood vulnerabilities.

In this paper, we show that the NIC suffers from an unexpected vulnerability, i.e., bitstream collisions, where semantically different images can be compressed to the same bitstream. Some sample collision images that we derived are illustrated in Fig. 1. For any target image x_{tgt} with compressed bitstream b_{tgt} , we can find adversarial images x_{adv} that are semantically different from x_{tgt} but compressed to the same bitstream b_{tgt} . The image x_{adv} can be perceptually similar to any arbitrary source image x_{src} .

For traditional codecs like JPEG, it is well understood that if two images produce similar compressed bitstreams, the images are likely perceptually similar, with minor differences in noise or high-frequency variations. This paper shows that no such guarantee is available for NIC. Since semantically different images may be compressed to identical bitstreams, this exposes a severe vulnerability in many applications. It

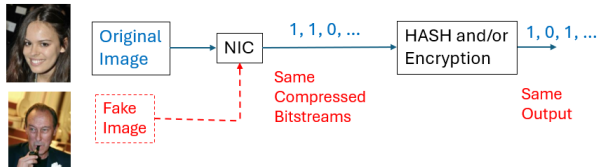


Figure 2. NIC with a collision vulnerability compromises cryptographic protocols.

is ambiguous at the decompressor side which image, x_{adv} or x_{tgt} , is the true uncompressed image. For example, in video surveillance or face recognition, the image is compressed and transmitted to some central processor for recognition. The collisions may lead to incorrect recognitions.

The most detrimental consequence is to cryptographic protocols that integrate NIC, as illustrated in Fig. 2. Cryptographic protocols used in digital signatures, digital IDs, blockchains, etc, may compress an image and then hash/encrypt the compressed bitstream (Menezes et al., 2018; Gelb & Metz, 2018). If NIC is applied, both the integrity and non-repudiation properties of the cryptographic protocols will be compromised due to NIC’s collision vulnerability. An attacker may replace the original image with fake images but still obtain the same hash/encryption output. The attacker may also argue that the image used in hash or encryption is not the original one.

This paper investigates the NIC collision vulnerability with the following contributions:

- We develop a Masked Gradient Descent (MGD) attack algorithm to generate collision images. To the best of our knowledge, this is the first time the collision vulnerability of NIC is discovered and demonstrated.
- We analyze the collision problem theoretically and propose a novel Limited Precision Defense (LPD) method that is simple to implement and can effectively mitigate the collision vulnerability.
- We evaluate the efficacy of the proposed attack and defense across multiple datasets, compression quality factors, and NIC model architectures.

The paper is organized as follows: Section 2 provides a literature review. Section 3 formulates the new attack algorithm and defense method. Section 4 presents the experiment results, and Section 5 concludes the paper. ¹

¹Our source code can be found at <https://github.com/neddaj/nicsec>.

2. Literature Review

2.1. Neural Image Compression

Using neural networks for image compression has attracted long-term research interests (Dony & Haykin, 1995; Cramer, 1998). Surveys of NIC as well as the current state-of-the-art can be found in (Ma et al., 2019; Yang et al., 2023; Jamil et al., 2023).

In the initial stage of deep learning-based NIC development, works dealt with the issues of non-differentiable quantization and rate estimation to enable end-to-end training of NIC models (Agustsson et al., 2017; Ballé et al., 2016c). Subsequent research shifted towards optimizing network architectures for efficient latent representation extraction and high-quality image reconstruction (Yang et al., 2020; Guo et al., 2021; Yang et al., 2021; Zhu et al., 2022; Gao et al., 2022; Strümpfer et al., 2022; Muckley et al., 2023). Recurrent neural networks, as employed in works such as (Toderici et al., 2017; 2015) demonstrated success in compressing residual information recursively. Generative models were used to learn the image distributions, achieving improved subjective quality at very low bit rates, as seen in (Rippel & Bourdev, 2017; Santurkar et al., 2018; Mentzer et al., 2020). Additionally, techniques such as (Ballé et al., 2018; Minnen et al., 2018; Cheng et al., 2020) focused on adaptive context models for entropy estimation to achieve the optimal tradeoff between reconstruction error and entropy.

2.2. Adversarial Machine Learning

Adversarial attacks can be classified as either untargeted or targeted. In an untargeted attack, the attacker aims to slightly change the input to the model, so that the model produces a wildly different output. In a targeted attack, the attacker changes the input to the model slightly to cause the model to generate a predefined output. Adversarial attacks can also be categorized based on the level of access the attacker has to the target model. In whitebox attacks (Szegedy, 2013; Madry, 2017; Carlini & Wagner, 2017), the attacker has complete knowledge of the model, including its architecture and parameters. On the other hand, blackbox attacks (Ilyas et al., 2018; Liu et al., 2019; Brendel et al., 2017; Chen et al., 2020) occur when the attacker has no access to the model’s inner workings, relying only on inputs and outputs. Blackbox attacks can be further divided into two types: soft-label attacks (Ilyas et al., 2018; Liu et al., 2019), where the model outputs continuous values like probabilities or logits, and hard-label attacks (Brendel et al., 2017; Chen et al., 2020), where the model provides only discrete decision labels. In this work, we will develop new targeted whitebox attacks to create collision images.

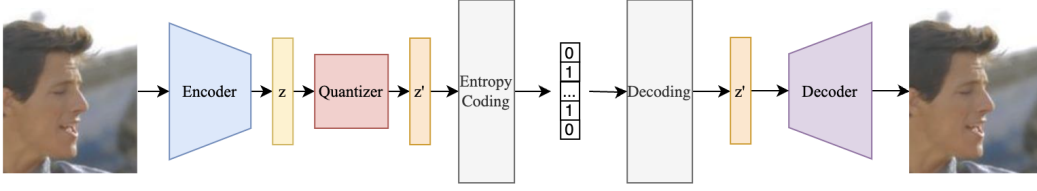


Figure 3. Standard Neural Image Compression and Decompression Pipeline

2.3. Adversarial Robustness of NIC

In contrast to the abundant literature on either NIC or adversarial machine learning, there is not much work done on NIC robustness. (Liu et al., 2023) demonstrated that the introduction of adversarial noise can lead to a substantial increase in the compressed bit rate. Additionally, (Chen & Ma, 2023) discovered that even the injection of minuscule amounts of adversarial noise can result in severe distortions in the reconstructed images. With the introduction of JPEG AI (Ascenso et al., 2023), there is now a standard for end-to-end JPEG compression methods. In response, (Kovalev et al., 2024) developed a novel methodology specifically designed to assess the robustness of JPEG models against adversarial attacks.

As far as we know, this work is the first to study the compressed bitstream collision problem.

3. Robustness of Neural Compression

3.1. NIC Model

We consider lossy compression as described in (Yang et al., 2023). The NIC models are inspired by the model of transform coding, in which an analysis transform f and a synthesis transform g are jointly optimized to compress/decompress an image with certain rate-distortion performance. As shown in Fig. 3, for an image x , f computes a continuous representation $z = f(x)$, which is then quantized to $z' = \lfloor z \rfloor$. Entropy coding is applied to create the compressed bitstream $b = e(z')$. The decoding process reverts the entropy coding to get z' from b , and the synthesis transform is subsequently applied to reconstruct the original image as $x' = g(z')$.

In traditional compression, the analysis and synthesis are conducted by orthogonal linear transformations such as discrete Fourier transform. NIC uses deep neural networks (DNNs) instead, where the analysis and synthesis transforms are typically replaced by encoder and decoder models based on Convolutional Neural Networks (CNNs) (Theis et al., 2017; Ballé et al., 2016b). The various components of the pipeline in Fig. 3 are jointly optimized over a rate-distortion objective, such as $\mathbb{E}[-\log_2 p(\lfloor f(x) \rfloor)] +$

$\lambda \mathbb{E}[\mathcal{D}(x, g(\lfloor f(x) \rfloor))]$, where \mathbb{E} is expectation, λ is the trade-off factor, $p(\lfloor f(x) \rfloor)$ measures the bit rate, and \mathcal{D} is a distance metric that measures the image distortion.

3.2. Threat Model

Consider a NIC model and an image x_{tgt} with its compressed bitstream b_{tgt} . The attacker’s objective is to create an image x_{adv} that is semantically different from x_{tgt} but is also compressed to the same bitstream b_{tgt} . We assume that the attacker has whitebox access to the NIC model, allowing full knowledge of the model architecture, parameters, and gradients. Additionally, x_{adv} should look like a normal image with added perturbations small enough. To guarantee this, one approach is for the attacker to select an image x_{src} that is completely different from x_{tgt} and gradually perturb the former so that its compressed bitstream converges to the latter’s bitstream. This is similar to the methodology of some targeted blackbox attacks (Ilyas et al., 2018).

3.3. Attacker’s Masked Gradient Descent (MGD) Algorithm for Collision Generation

Starting from an image x_{src} , the attacker’s goal is to create x_{adv} so that it has the same bitstream as x_{tgt} , specifically, $b_{adv} = b_{tgt}$, or $e(\lfloor f(x_{src}) \rfloor) = e(\lfloor f(x_{tgt}) \rfloor)$. This could be achieved via the optimization

$$x_{adv} = \arg \min_x \|e(\lfloor f(x) \rfloor) - e(\lfloor f(x_{tgt}) \rfloor)\|, \quad (1)$$

where $\|\cdot\|$ can be some norm or Hamming distance, and x is initialized as x_{src} to ensure x_{adv} is semantically different from x_{tgt} . Unfortunately, the quantization and entropy encoding procedures make the gradient optimization of (1) challenging, if not impossible.

Observing that the quantization and entropy encoding used in NICs are conventional signal processing tasks that discard very small signal variations only, we propose to skip them and directly minimize the distance between the CNN encoder’s output logits $f(x_{adv})$ and $f(x_{tgt})$, which gives

$$x_{adv} = \arg \min_x \|f(x) - f(x_{tgt})\|. \quad (2)$$

If the optimized loss $\mathcal{L}(x_{adv}) = \|f(x_{adv}) - f(x_{tgt})\|$ is

small enough, the bitstreams of x_{adv} and x_{tgt} will become identical.

The new challenge is that optimizing (2) directly using gradient descent algorithm, or variations like Projected Gradient Descent (PGD) (Madry, 2017) or the algorithm of (Carlini & Wagner, 2017), largely fails. They either do not converge to a loss small enough for bitstream collision, or converge to $x_{adv} \approx x_{tgt}$, i.e., the adversarial image becomes just the target image. Through experiments, we find that when a patch of the adversarial image x_{adv} was edited, a corresponding, similarly sized patch of the decompressed adversarial image $g(\lfloor f(x_{adv}) \rfloor)$ was also changed. This indicated that each pixel that was changed in x_{adv} affected the corresponding pixel in $g(\lfloor f(x_{adv}) \rfloor)$, as well as a few pixels in its immediate vicinity. This meant that we could not freely run optimization on the entire image x_{adv} as the resulting perturbation would cause x_{adv} to look exactly like x_{tgt} .

Surprisingly, we find that the challenge can be resolved by applying a simple masking technique to the gradients. The role of the mask is just to set many gradient elements to zero before using the gradient to update the image. This allows the majority of the pixels in the image x_{adv} to remain unchanged. Only some pixels in the image are allowed to be perturbed.

Specifically, we use what we call a *dot mask* where a fixed portion of pixels, separated by a certain rows and columns, are allowed to be perturbed by the gradient. The dot mask function is formulated as

$$\mathcal{M}(g(h, w)) = \begin{cases} g(h, w), & \text{for } h = i\Delta_h + h_0, \\ & w = i\Delta_w + w_0, \\ & i = 0, 1, \dots; \\ 0, & \text{else} \end{cases} \quad (3)$$

where $g(h, w)$ is the gradient of the image x_{adv} at height h and width w , Δ_h and Δ_w are the stepsizes or strides across the height and width, whereas h_0 and w_0 are initial shiftings. The optimization of (2) can thus be conducted by the masked gradient (3) as follows:

$$x \leftarrow x - \mu \mathcal{M} \left(\frac{\partial \|f(x) - f(x_{tgt})\|}{\partial x} \right) \quad (4)$$

where $\mathcal{L}'(x) = \partial \|f(x) - f(x_{tgt})\| / \partial x$ is the gradient of the loss with respect to x .

The new attack algorithm is outlined in Algorithm 1. Because our main objective is to generate collision images, not enhance image quality, we do not apply any constraints over image distortions. Instead, the image distortion is indirectly suppressed via the early-stopping technique. The iterative optimization stops immediately whenever the bitstream collision occurs.

One may suspect that reducing Δ_h and Δ_w to 1 would improve the attack's effectiveness by allowing the adversarial

Algorithm 1 MGD: Masked Gradient Descent Algorithm

Initialization: Given total iteration I , x_{tgt} and its bitstream b_{tgt} , initialize $x = x_{src}$.

For $i = 0, 1, \dots, I - 1$, **do**

- Update (4) with respect to (2) and (3),
 - Compare the new x 's compressed bitstream b with b_{tgt} . Stop and output $x_{adv} = x$ if $b = b_{tgt}$.
-

perturbation to induce more change in the image. However, it would cause x_{adv} to converge to x_{tgt} instead of a perceptually different image. Therefore, it is critical to choose appropriate mask parameters as it helps to sufficiently maintain the semantic properties of the image x_{src} while allowing the attack to work sufficiently well. In practice, we find the attack to work best when we separate the dots horizontally by $\Delta_w = 1$ pixel and vertically by $\Delta_h = 3$ pixels. The shiftings can be simply set as $h_0 = w_0 = 0$.

Although we use a dot mask, any mask that distributes the perturbations throughout the image such that the image retains its semantic properties and the output converges to that of the target image would work. In addition, any loss functions that reduce the difference between $f(x_{adv})$ and $f(x_{tgt})$ would also work under the mask operation. We tried both mean square error and Cosine Similarity (CS), and found either of them, or their combination such as the following, worked well

$$\mathcal{L}(x) = \|f(x) - f(x_{tgt})\| + \frac{1}{2} [1 - CS(x, x_{tgt})] \quad (5)$$

where $CS(a, b) = \frac{a \cdot b}{\|a\| \|b\|}$.

3.4. NIC's Defense: A Limited-Precision Defense (LPD) Mechanism

Various common defense mechanisms applied in robust machine learning can be explored to mitigate NIC's collision vulnerability, such as the adversarial training used in (Chen & Ma, 2023). Nevertheless, we are more interested in the following NIC-specific mechanism, which we call *Limited-Precision Defense (LPD)*. It exploits a special characteristic of NIC, i.e., sensitivity to small perturbations. It is much simpler to implement and is also very effective.

In our initial experiments, we observed a surprising phenomenon: for the attack to work, we needed to disable the TF32 tensor cores on our GPUs; otherwise we could not get any collisions. Through careful study, we found that the reduced precision of TF32 interfered with the convergence of Algorithm 1. Even though the loss $\mathcal{L}(x)$ can still be as small as in the case without using TF32, the compressed bitstream of the adversarial image could hardly be equal to

that of the target image. The reason is that the compressed bitstream is extremely sensitive to even minor variations in the latent representations.

Drawing from this observation, we propose the unique *LPD* method, i.e., converting some latent tensors and/or some model parameters to half-precision. If a NIC model is developed with float32, then we change some data to float16. It turns out that this simple change can effectively mitigate the attack algorithms.

This method can be directly applied in real NIC applications. Especially for the crypto application shown in Fig. 2, the limited-precision implementation of NIC does not affect the normal operation of the crypto-chain. Each unique image will still lead to a fixed and unique compressed bitstream. The adversary, or anyone else, can recreate this compressed bitstream using the same limited-precision implementation. However, if high-precision implementation is used, the generated bitstream will be different from the true one. Without a high-precision implementation, the attack algorithms can hardly converge to valid collision images.

3.5. Theoretical Bounds of the Distance between Collision Images

To be considered as a vulnerability, collision images must be semantically different, or the distance between the images must be large. In this section, we derive the bounds of such distances between collision images.

Recall the encoding function f (see Section 3.1 and Fig. 3) that transforms an image x to their latent embeddings (or logits) $z = f(x)$. We skip the details of the quantization and entropy encoding, but model the data compression procedure as follows. Let

$$z = z_b + z_v \quad (6)$$

where z_b is a vector consisting of all the values of z whose magnitudes are larger than a threshold γ , while z_v is a vector consisting of all the values with magnitude less than the threshold γ . The data compression is to discard z_v while keeping just z_b . With this compression model, the compression ratio R , defined as the ratio between the total number of elements in z and the number of elements in z_b , becomes

$$R = \frac{1}{\mathbb{P}[|z| > \gamma]} = \frac{1}{2 \int_{\gamma}^{\infty} p(z) dz} \quad (7)$$

where $p(z)$ is the distribution of z .

Theorem 1. *Assume the elements of images x_{tgt} and x_{adv} are independent with identical normal distribution $\mathcal{N}(0, 1)$. In conventional compression with orthogonal transform f , if x_{tgt} and x_{adv} are compressed to the same bitstream, then their per-pixel distance, defined as $\mathcal{D}_c(x_{tgt}, x_{adv}) \triangleq$*

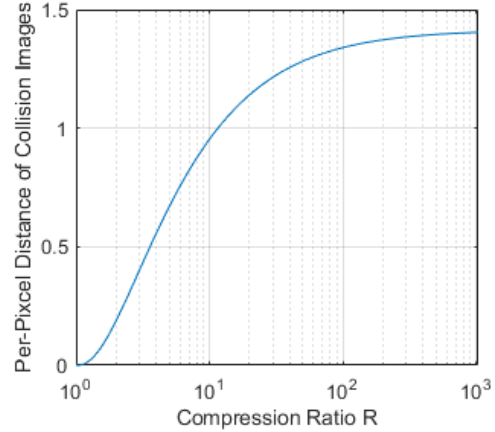


Figure 4. Theoretical limit of collision image distance as a function of compression ratio for conventional compressors with orthogonal f .

$\{\mathbb{E}[\|x_{tgt} - x_{adv}\|^2/M]\}^{1/2}$ with L_2 norm and total M pixels, is bounded by $\sqrt{2}$, i.e.

$$\mathcal{D}_c(x_{tgt}, x_{adv}) \leq \sqrt{2}. \quad (8)$$

Proof: If f is an orthogonal transform such as discrete Fourier transform (DFT) or singular value decomposition (SVD), then the elements of $z_{tgt} = f(x_{tgt})$ and $z_{adv} = f(x_{adv})$ are also distributed as $\mathcal{N}(0, 1)$. From (6), we have $z_{adv} = z_{adv,b} + z_{adv,v}$ and $z_{tgt} = z_{tgt,b} + z_{tgt,v}$. We also have $z_{adv,b} = z_{tgt,b}$ because they are compressed to the same bitstream. The distance square between the two images x_{adv} and x_{tgt} can be deduced as

$$\begin{aligned} \mathcal{D}_c^2(x_{tgt}, x_{adv}) &= \mathbb{E}[\|z_{tgt} - z_{adv}\|^2/M] \\ &= \mathbb{E}[\|z_{tgt,v} - z_{adv,v}\|^2/M] \end{aligned} \quad (9)$$

Because all the elements of $z_{tgt,v}$ and $z_{adv,v}$ (each of them has $M(1 - 1/R)$ elements) are less than γ , we have

$$\mathcal{D}_c^2(x_{tgt}, x_{adv}) = \frac{R-1}{R} \int_{-\gamma}^{\gamma} \int_{-\gamma}^{\gamma} (x-y)^2 p(x)p(y) dx dy \quad (10)$$

where both $p(x)$ and $p(y)$ are $\mathcal{N}(0, 1)$. Next, to prove (8), we use the property that \mathcal{D}_c increases monotonically with γ . Let $\gamma = \infty$, we can calculate (10) to be 2. \square

We have verified Theorem 1 via simulations. We derived closed-form solutions to (7) and (10), and plotted the distance curve in Fig. 4. It can be seen that the distance increases with the compression ratio up to the bound $\sqrt{2}$.

For NIC, although accurate distance is unavailable, we can still derive useful information about the bounds.

Theorem 2. *Different from conventional deep model robustness that requires a small Lipschitz constant, large Lipschitz constant is helpful to collision mitigation.*

Proof. Assume f is a deep model that is Lipschitz continuous (Fazlyab et al., 2019) with Lipschitz constant L , i.e. $\|f(x_{tgt}) - f(x_{adv})\| \leq L\|x_{tgt} - x_{adv}\|$. Following (9), the distance square can be calculated as follows

$$\begin{aligned} \mathcal{D}_n^2(x_{tgt}, x_{adv}) &= \mathbb{E} [\|x_{tgt} - x_{adv}\|^2/M] \\ &\geq \frac{1}{L^2} \mathbb{E} [\|f(x_{tgt}) - f(x_{adv})\|^2/M] \\ &= \frac{1}{L^2} \mathbb{E} [\|z_{tgt,v} - z_{adv,v}\|^2/M]. \end{aligned} \quad (11)$$

This means that the lower bound of the distance is decreased by L . Increasing L can make the NIC more robust to collisions, which is different from conventional deep model robustness requirements. \square

The upper bound of the distance is more interesting than the lower bound. To derive the upper bound, instead of the Lipschitz constant, we need to consider the following new constant C which we call *contraction constant*

$$C = \max_{x,y} \frac{\|x - y\|}{\|f(x) - f(y)\|}. \quad (12)$$

Theorem 3. Assume f 's output is normalized to $\mathcal{N}(0, 1)$ in NICs, then $\mathcal{D}_n(x_{tgt}, x_{adv}) \leq \sqrt{2}C$.

Proof. The definition (12) means

$$\|x_{tgt} - x_{adv}\| \leq C\|f(x_{tgt}) - f(x_{adv})\|. \quad (13)$$

Then, with a similar procedure as (11), we can get

$$\mathcal{D}_n^2(x_{tgt}, x_{adv}) \leq C^2 \mathbb{E} [\|z_{tgt,v} - z_{adv,v}\|^2/M]. \quad (14)$$

Following (10), we can easily prove this theorem. \square

Theorem 3 shows that the upper bound of the distance is C times higher in NICs than in conventional compressors (10). For more robust NIC, we need to look for f with a small C . This can be a new mitigation method to explore in the future.

4. Experimental Results and Discussion

4.1. Experiment Settings

We evaluated our proposed **MGD** attack algorithm and the **LPD** defense method using three distinct datasets: CelebA, ImageNet, and the Kodak dataset, with all images resized to 256×256 pixels. Additionally, we compared the proposed MGD attack algorithm against two standard attack algorithms: the Projected Gradient Descent (**PGD**) attack algorithm (Madry, 2017) and the Carlini-Wagner (**CW**) attack algorithm (Carlini & Wagner, 2017).

Most neural compression algorithms are significantly more computationally intensive than traditional codecs and this

may hinder their adoption in practice. As a result, our work emphasizes compressors that deliver strong performance while utilizing fewer parameters. In our experiments, we adopted three NIC models that satisfy this criterion: two Factorized Prior models (**FP-GDN** and **FP-ReLU**) and the Scale Hyperprior model (**SH**) presented in (Ballé et al., 2018). For Factorized Prior models, we used two implementations: the model using the Generalized Divisive Normalization (GDN) layers (Ballé et al., 2016a) and the one using ReLU layers instead of GDN layers. For comparison, we also evaluated the robustness of JPEG under the above attacks.

For the Factorized Prior models, we ran attack optimization for at most $I = 5,000$ iterations, whereas for the Scale Hyperprior model, we ran optimization for at most $I = 20,000$ iterations. In both cases, we used the Adam optimizer (Kingma, 2014) with an initial learning rate of 0.03 to perform optimization. We varied the learning rate throughout the attack with a Cosine Annealing learning rate scheduler (Loshchilov & Hutter, 2022).

To measure the similarity between two sets of N -bit bitstreams we calculate the normalized Hamming distance as

$$H(b_1, b_2) = \frac{1}{N} \sum_{n=1}^N \mathbb{I}(b_1(n) - b_2(n)) \quad (15)$$

where $\mathbb{I}(\cdot)$ is the indicator function $\mathbb{I}(x) = 1$ if $x \neq 0$ and 0 if $x = 0$. Then, given the Hamming distance, the attack success rate (ASR) is the percentage of adversarial images x_{adv} whose compressed bitstream has a Hamming distance of 0 when compared with the compressed bitstream of the target image x_{tgt} . This can be written more formally as

$$ASR = \frac{1}{M} \sum_{m=1}^M (1 - \mathbb{I}(H(b_{tgt}, b_{adv}^m))) \quad (16)$$

where b_{tgt} is the compressed bitstream of the target image x_{tgt} and b_{adv}^m is the compressed bitstream of the m th adversarial image x_{adv} . We also tracked the quality of the adversarial images x_{adv} using per-pixel L_2 norm

$$L_2(x, y) = \sqrt{\frac{1}{M} \sum_{m=1}^M (x_m - y_m)^2} \quad (17)$$

where x and y are images consisting of M pixels.

4.2. Performance of MGD Attack Algorithm

In this set of experiments, we perturb source images x_{src} and change them into adversarial images x_{adv} that have the compressed bitstreams exactly the same as that of the target image x_{tgt} . The ASR values we obtained are shown in Table 1. We can easily see that bitstream collision is

Attack Alg		MGD (ours)			PGD			CW		
QF	NIC	CelebA	ImageNet	Kodak	CelebA	ImageNet	Kodak	CelebA	ImageNet	Kodak
1	FP-GDN	1.00	1.00	1.00	0	0	0	0	0	0
	FP-ReLU	1.00	1.00	1.00	0	0	0	0	0	0
	SH	0.19	0.05	0.33	0	0	0	0	0	0
2	FP-GDN	1.00	1.00	1.00	0	0	0	0	0	0
	FP-ReLU	1.00	1.00	1.00	0	0	0	0	0	0
	SH	0.11	0.04	0.17	0	0	0	0	0	0
3	FP-GDN	1.00	1.00	1.00	0	0	0	0	0	0
	FP-ReLU	1.00	1.00	1.00	0	0	0	0	0	0
	SH	0	0	0	0	0	0	0	0	0
4	FP-GDN	0.32	0.94	0.92	0	0	0	0	0	0
	FP-ReLU	0.32	0.94	0.92	0	0	0	0	0	0
	SH	0	0	0	0	0	0	0	0	0
≥ 5	FP-GDN	0	0	0	0	0	0	0	0	0
	FP-ReLU	0	0	0	0	0	0	0	0	0
	SH	0	0	0	0	0	0	0	0	0
any	JPEG	0	0	0	0	0	0	0	0	0

Table 1. ASR of 3 attack algorithms (MGD, PGD, CW) applied to 3 NIC Models (FP-GDN, FP-ReLU, SH) plus a JPEG model over 3 datasets (CelebA, ImageNet, Kodak).

a real vulnerability to NICs. Our proposed MGD easily generated collision images with extremely high probability. In comparison, JPEG compression was extremely robust to bitstream collision attacks, as no valid collision image was obtained at all.

We also observe that NICs appeared robust against conventional attack algorithms PGD and CW. In other words, the proposed MGD attack was more powerful than PGD and CW. SH was relatively more robust than FP-GDN and FP-ReLU. Some extra observations about the PGD performance are in Appendix B.

There was a strong relationship between the quality factor (QF) of the compressor and the efficacy of the attack. As the QF increases, the length of the compressed bitstream increases or the compression ratio decreases. This effect can be seen in Fig. 5. For NICs to have higher compression ratio than JPEG, the QF should be less than 5. But for small QF, bitstream collision becomes a severe vulnerability.

Table 2 shows the quality of the successful collision images x_{adv} generated by our MGD algorithm, where $L_2(x_{adv}, x_{tgt})$ is the distance between x_{adv} and the target image x_{tgt} , and $L_2(x_{adv}, x_{src})$ is the distance between x_{adv} and x_{src} . We can see from the table that $L_2(x_{adv}, x_{tgt})$ was always very big, which means the adversarial images were perceptually different from the target image, even though their compressed bitstreams were the same. The $L_2(x_{adv}, x_{src})$ values were relatively smaller, indicating that the adversarial images were noise-perturbed versions from the source images. Extra perceptual data are shown in Appendix A and image samples are shown in Appendix C.

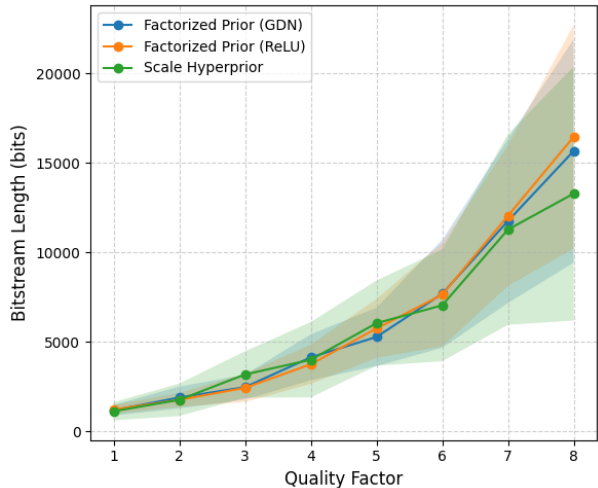


Figure 5. Compressed bitstream length vs Quality Factor (QF) over the three datasets. Note that bitstream length 10000 equals to compression ratio $R = 150$, which is approximately the JPEG compression ratio of the datasets.

4.3. Transferability of MGD Attacks

We evaluated the transferability of adversarial images between NIC models. Specifically, we ran the attacks on a model to generate x_{adv} that collided with x_{tgt} . Then, we checked if x_{adv} still collided with x_{tgt} on a different model. The results of these experiments are available in Tables 3 and 4. In the tables, the first column describes the models that the attack was conducted on to generate x_{adv} , and the

QF	NIC Model	$L_2(x_{adv}, x_{tgt})$			$L_2(x_{adv}, x_{src})$		
		CelebA	ImageNet	Kodak	CelebA	ImageNet	Kodak
1	FP-GDN	0.88±0.12	0.80±0.08	0.71±0.08	0.62±0.04	0.53±0.04	0.57±0.08
	FP-ReLU	0.90±0.14	0.78±0.08,	0.71±0.14	0.68±0.08	0.60±0.06	0.61±0.10
	SH	1.89±0.32	1.35±0.29	0.98±0.16	1.53±0.28	1.01±0.19	0.74±0.14
2	FP-GDN	0.93±0.08	0.89±0.12	0.90±0.13	0.66±0.08	0.62±0.04	0.72±0.16
	FP-ReLU	0.87±0.12	0.82±0.14	0.89±0.12	0.68±0.09	0.64±0.12	0.71±0.12
	SH	1.80±0.34	1.48±0.27	1.36±0.24	1.31±0.30	1.02±0.18	1.05±0.26
3	FP-GDN	0.93±0.12	0.93±0.08	0.76±0.11	0.59±0.08	0.61±0.05	0.55±0.08
	FP-ReLU	0.93±0.12	0.86±0.16	0.91±0.14	0.62±0.08	0.67±0.12	0.70±0.18
	SH	-	-	-	-	-	-
4	FP-GDN	1.15±0.12,	1.11±0.12,	0.98±0.15,	0.87±0.08	0.88±0.08	0.80±0.13
	FP-ReLU	1.06±0.12,	0.99±0.14,	1.08±0.11,	0.89±0.11	0.79±0.12	0.80±0.10
	SH	-	-	-	-	-	-

Table 2. L_2 distance of **successful** adversarial images x_{adv} from x_{tgt} or x_{src} . Each entry $a \pm b$ means average L_2 distance a with standard deviation b . The dash ‘-’ means no successful x_{adv} found.

NIC Model	FP-GDN	FP-ReLU	SH
FP-GDN	-	96.7%	0%
FP-ReLU	95.6%	-	0%
SH	0%	0%	-

Table 3. Percentage of adversarial images that transfer between NIC models. CelebA dataset.

NIC Model	FP-GDN	FP-ReLU	SH
FP-GDN	-	90.3%	0%
FP-ReLU	89.9%	-	0%
SH	0%	0%	-

Table 4. Percentage of adversarial images that transfer between NIC models. ImageNet dataset.

first row are the models that x_{adv} was evaluated on. Within the Factorized Prior family of models, the transfer attacks were essentially 100% successful for each dataset that we evaluated on. While the attacks were transferrable within the Factorized Prior family of models, they were not transferrable between either of the Factorized Prior models and the Scale Hyperprior model.

4.4. Defense Performance of LPD

We implemented the LPD defense to all the three NIC models (FP-GDN, FP-ReLU, SH) with quality factor 1, and applied the proposed MGD attack. The ASR data are shown in Table 5. Prior to applying the defense, the attacks had a very high success rate, especially on the Factorized Prior models which had 100% attack successful rate (Table 1). But our defense method reduced the ASR to 0 across all models and datasets that we tested. This demonstrates that the proposed defense method was extremely effective.

NIC Model	CelebA	ImageNet
FP-GDN	0	0
FP-ReLU	0	0
SH	0	0

Table 5. ASR after the LPD defense method is applied.

5. Conclusion

In this paper, we demonstrate that neural image compression (NIC) suffers from a unique vulnerability, bitstream collision, that conventional image compression algorithms such as JPEG do not. A new attack algorithm called Masked Gradient Descent (MGD) algorithm is developed to generate collision images that are perceptually different but have the identical compressed bitstreams. Surprisingly, this vulnerability may be mitigated by a simple Limited-Precision Defense (LPD) method, which implements some portions of the NIC models with limited resolution. Extensive experiments are conducted to verify the MGD algorithm and the LPD method. Considering the important role played by data compression in many security-critical applications, the collision vulnerability should be explored thoroughly before the real adoption of NIC technology.

References

- Agustsson, E., Mentzer, F., Tschannen, M., Cavigelli, L., Timofte, R., Benini, L., and Gool, L. V. Soft-to-hard vector quantization for end-to-end learning compressible representations. *Advances in neural information processing systems*, 30, 2017.
- Ascenso, J., Alshina, E., and Ebrahimi, T. The jpeg ai standard: Providing efficient human and machine visual data consumption. *Ieee Multimedia*, 30(1):100–111, 2023.

- Ballé, J., Laparra, V., and Simoncelli, E. P. Density modeling of images using a generalized normalization transformation. In *4th International Conference on Learning Representations, ICLR 2016*, 2016a.
- Ballé, J., Laparra, V., and Simoncelli, E. P. End-to-end optimization of nonlinear transform codes for perceptual quality. In *2016 Picture Coding Symposium (PCS)*, pp. 1–5. IEEE, 2016b.
- Ballé, J., Laparra, V., and Simoncelli, E. P. End-to-end optimized image compression. *arXiv preprint arXiv:1611.01704*, 2016c.
- Ballé, J., Minnen, D., Singh, S., Hwang, S. J., and Johnston, N. Variational image compression with a scale hyperprior. In *International Conference on Learning Representations*, 2018.
- Bastug, E., Bennis, M., Médard, M., and Debbah, M. Toward interconnected virtual reality: Opportunities, challenges, and enablers. *IEEE Communications Magazine*, 55(6):110–117, 2017.
- Brendel, W., Rauber, J., and Bethge, M. Decision-based adversarial attacks: Reliable attacks against black-box machine learning models. *arXiv preprint arXiv:1712.04248*, 2017.
- Carlini, N. and Wagner, D. Towards evaluating the robustness of neural networks. In *2017 IEEE Symposium on Security and Privacy (SP)*, pp. 39–57. Ieee, 2017.
- Chen, J., Jordan, M. I., and Wainwright, M. J. Hop-skipjumpattack: A query-efficient decision-based attack. In *2020 IEEE Symposium on Security and Privacy (SP)*, pp. 1277–1294. IEEE, 2020.
- Chen, T. and Ma, Z. Toward robust neural image compression: Adversarial attack and model finetuning. *IEEE Transactions on Circuits and Systems for Video Technology*, 33(12):7842–7856, 2023.
- Cheng, Z., Sun, H., Takeuchi, M., and Katto, J. Learned image compression with discretized gaussian mixture likelihoods and attention modules. In *Proceedings of the IEEE/CVF conference on computer vision and pattern recognition*, pp. 7939–7948, 2020.
- Cramer, C. Neural networks for image and video compression: A review. *European journal of operational research*, 108(2):266–282, 1998.
- Dony, R. D. and Haykin, S. Neural network approaches to image compression. *Proceedings of the IEEE*, 83(2): 288–303, 1995.
- Fazlyab, M., Robey, A., Hassani, H., Morari, M., and Pappas, G. Efficient and accurate estimation of lipschitz constants for deep neural networks. *Advances in neural information processing systems*, 32, 2019.
- Gao, C., Xu, T., He, D., Wang, Y., and Qin, H. Flexible neural image compression via code editing. *Advances in Neural Information Processing Systems*, 35:12184–12196, 2022.
- Gelb, A. and Metz, A. D. *Identification revolution: Can digital ID be harnessed for development?* Brookings Institution Press, 2018.
- Guo, Z., Zhang, Z., Feng, R., and Chen, Z. Soft then hard: Rethinking the quantization in neural image compression. In *International Conference on Machine Learning*, pp. 3920–3929. PMLR, 2021.
- Ilyas, A., Engstrom, L., Athalye, A., and Lin, J. Black-box adversarial attacks with limited queries and information. In *International conference on machine learning*, pp. 2137–2146. PMLR, 2018.
- Jamil, S., Piran, M. J., Rahman, M., and Kwon, O.-J. Learning-driven lossy image compression: A comprehensive survey. *Engineering Applications of Artificial Intelligence*, 123:106361, 2023.
- Kingma, D. P. Adam: A method for stochastic optimization. *arXiv preprint arXiv:1412.6980*, 2014.
- Kovalev, E., Bychkov, G., Abud, K., Gushchin, A., Chistyakova, A., Lavrushkin, S., Vatolin, D., and Antsiferova, A. Exploring adversarial robustness of jpeg ai: methodology, comparison and new methods. *arXiv preprint arXiv:2411.11795*, 2024.
- Liu, K., Wu, D., Wu, Y., Wang, Y., Feng, D., Tan, B., and Garg, S. Manipulation attacks on learned image compression. *IEEE Transactions on Artificial Intelligence*, 2023.
- Liu, S., Chen, P.-Y., Chen, X., and Hong, M. signsgd via zeroth-order oracle. In *International Conference on Learning Representations*, 2019.
- Loshchilov, I. and Hutter, F. Sgdr: Stochastic gradient descent with warm restarts. In *International Conference on Learning Representations*, 2022.
- Ma, S., Zhang, X., Jia, C., Zhao, Z., Wang, S., and Wang, S. Image and video compression with neural networks: A review. *IEEE Transactions on Circuits and Systems for Video Technology*, 30(6):1683–1698, 2019.
- Madry, A. Towards deep learning models resistant to adversarial attacks. *arXiv preprint arXiv:1706.06083*, 2017.

- Menezes, A. J., Van Oorschot, P. C., and Vanstone, S. A. *Handbook of applied cryptography*. CRC press, 2018.
- Mentzer, F., Toderici, G. D., Tschannen, M., and Agustsson, E. High-fidelity generative image compression. *Advances in Neural Information Processing Systems*, 33:11913–11924, 2020.
- Minnen, D., Ballé, J., and Toderici, G. D. Joint autoregressive and hierarchical priors for learned image compression. *Advances in neural information processing systems*, 31, 2018.
- Muckley, M. J., El-Nouby, A., Ullrich, K., Jégou, H., and Verbeek, J. Improving statistical fidelity for neural image compression with implicit local likelihood models. In *International Conference on Machine Learning*, pp. 25426–25443. PMLR, 2023.
- Rippel, O. and Bourdev, L. Real-time adaptive image compression. In *International Conference on Machine Learning*, pp. 2922–2930. PMLR, 2017.
- Santurkar, S., Budden, D., and Shavit, N. Generative compression. In *2018 Picture Coding Symposium (PCS)*, pp. 258–262. IEEE, 2018.
- Strümler, Y., Postels, J., Yang, R., Gool, L. V., and Tombari, F. Implicit neural representations for image compression. In *European Conference on Computer Vision*, pp. 74–91. Springer, 2022.
- Szegedy, C. Intriguing properties of neural networks. *arXiv preprint arXiv:1312.6199*, 2013.
- Theis, L., Shi, W., Cunningham, A., and Huszár, F. Lossy image compression with compressive autoencoders. *arXiv preprint arXiv:1703.00395*, 2017.
- Toderici, G., O’Malley, S. M., Hwang, S. J., Vincent, D., Minnen, D., Baluja, S., Covell, M., and Sukthankar, R. Variable rate image compression with recurrent neural networks. *arXiv preprint arXiv:1511.06085*, 2015.
- Toderici, G., Vincent, D., Johnston, N., Jin Hwang, S., Minnen, D., Shor, J., and Covell, M. Full resolution image compression with recurrent neural networks. In *Proceedings of the IEEE conference on Computer Vision and Pattern Recognition*, pp. 5306–5314, 2017.
- Yang, F., Herranz, L., Cheng, Y., and Mozerov, M. G. Slimmable compressive autoencoders for practical neural image compression. In *Proceedings of the IEEE/CVF Conference on Computer Vision and Pattern Recognition*, pp. 4998–5007, 2021.
- Yang, Y., Bamler, R., and Mandt, S. Improving inference for neural image compression. *Advances in Neural Information Processing Systems*, 33:573–584, 2020.
- Yang, Y., Mandt, S., Theis, L., et al. An introduction to neural data compression. *Foundations and Trends® in Computer Graphics and Vision*, 15(2):113–200, 2023.
- Zhu, X., Song, J., Gao, L., Zheng, F., and Shen, H. T. Unified multivariate gaussian mixture for efficient neural image compression. In *Proceedings of the IEEE/CVF Conference on Computer Vision and Pattern Recognition*, pp. 17612–17621, 2022.

A. MS-SSIM of Generated Images

Table 2 shows the L_2 distance of the *successful* adversarial images. For a better representation of the perceptual similarity, the Multi-Scale Structural Similarity Index Measure (MS-SSIM) might be a more preferred performance measure. Table 6 shows the MS-SSIM of all the adversarial images, either successful or not, that we generated in our experiments. The data in the column of $\text{MS-SSIM}(x_{adv}, x_{tgt})$ are small in general, indicating that the adversarial images x_{adv} were semantically different to x_{tgt} . On the other hand, the data in the column of $\text{MS-SSIM}(x_{adv}, x_{src})$ are large in general, meaning the adversarial images x_{adv} were semantically similar to x_{src} . In addition, from the column of $\text{MS-SSIM}(x_{adv}, x_{src})$, the perturbation level of PGD and CW was similar as MGD but still failed (because the ASRs of PGD and CW were 0 in Table 1). Therefore, MGD is a more superior attack algorithm than the other two.

Attacks	MS-SSIM(x_{adv}, x_{tgt})			MS-SSIM(x_{adv}, x_{src})		
	MGD (ours)	PGD	CW	MGD (ours)	PGD	CW
FP-GDN	0.14±0.04	0.22±0.13	0.41±0.08	0.75±0.11	0.74±0.07	0.69±0.06
FP-ReLU	0.11±0.03	0.24±0.11	0.43±0.08	0.73±0.07	0.75±0.08	0.67±0.07
SH	0.18±0.03	0.27±0.10	0.40±0.06	0.71±0.03	0.75±0.05	0.70±0.02

Table 6. Average MS-SSIM of all the images x_{adv} , whether successful or unsuccessful collisions, for all the quality factors and all the three datasets.

B. Further exploration of the effectiveness of PGD attack

When experimenting with the PGD attack algorithm to generate collision images in Section 4.2, we constrained the perturbations within a $\epsilon = 0.1$ ball to minimize distortion. However, this led to poor ASR for PGD across the board. We observed that increasing the magnitude of allowable perturbations caused the ASR to increase, but it also caused an increase of distortion. This effect is illustrated in Fig. 6. When the ASR is increased from 0 to 0.05, the distortion of the adversarial image is already reduce to having MS-SSIM of 0.02 only. Note that the MS-SSIM is the Multi-Scale Structural Similarity Index Measure between x_{adv} and x_{src} . As a result, the PGD attack algorithm is not competitive to the proposed MGD attack algorithm.

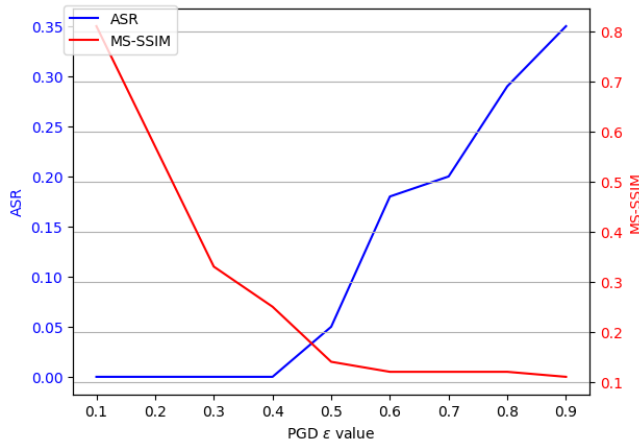


Figure 6. Evolution of ASR and MS-SSIM as ϵ changes in PGD

C. Sample Adversarial Images

Figs. 7-15 show samples of source images x_{src} , adversarial images x_{adv} , and target images x_{tgt} , as well as their compressed bitstreams. All the images x_{adv} have bitstream collisions to the target images.



Figure 7. Images from the CelebA dataset with their corresponding compressed bitstreams generated with the Scale Hyperprior (SH) model. Source Images and their compressed bitstreams (left). Adversarial Images and their compressed bitstreams (center). Target Image and its compressed bitstream (right).



Figure 8. Images from the ImageNet dataset with their corresponding compressed bitstreams generated with the Scale Hyperprior (SH) model. Source Images and their compressed bitstreams (left). Adversarial Images and their compressed bitstreams (center). Target Image and its compressed bitstream (right).



Figure 9. Images from the Kodak dataset with their corresponding compressed bitstreams generated with the Scale Hyperprior (SH) model. Source Images and their compressed bitstreams (left). Adversarial Images and their compressed bitstreams (center). Target Image and its compressed bitstream (right).

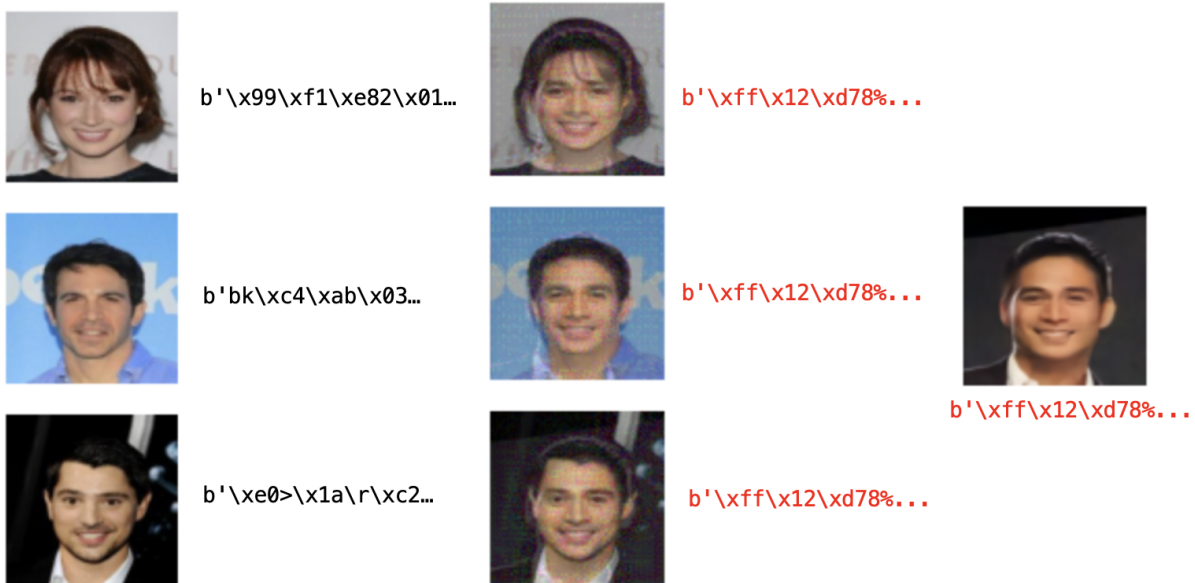


Figure 10. Images from the CelebA dataset with their corresponding compressed bitstreams generated with the Factorized Prior (ReLU) model. Source Images and their compressed bitstreams (left). Adversarial Images and their compressed bitstreams (center). Target Image and its compressed bitstream (right).



Figure 11. Images from the ImageNet dataset with their corresponding compressed bitstreams generated with the Factorized Prior (ReLU) model. Source Images and their compressed bitstreams (left). Adversarial Images and their compressed bitstreams (center). Target Image and its compressed bitstream (right).



Figure 12. Images from the Kodak dataset with their corresponding compressed bitstreams generated with the Factorized Prior (ReLU) model. Source Images and their compressed bitstreams (left). Adversarial Images and their compressed bitstreams (center). Target Image and its compressed bitstream (right).



Figure 13. Images from the CelebA dataset with their corresponding compressed bitstreams generated with the Factorized Prior (GDN) model. Source Images and their compressed bitstreams (left). Adversarial Images and their compressed bitstreams (center). Target Image and its compressed bitstream (right).



Figure 14. Images from the Imagenet dataset with their corresponding compressed bitstreams generated with the Factorized Prior (GDN) model. Source Images and their compressed bitstreams (left). Adversarial Images and their compressed bitstreams (center). Target Image and its compressed bitstream (right).



Figure 15. Images from the Kodak dataset with their corresponding compressed bitstreams generated with the Factorized Prior (GDN) model. Source Images and their compressed bitstreams (left). Adversarial Images and their compressed bitstreams (center). Target Image and its compressed bitstream (right).